Computers and Concrete, *Vol. 22, No. 2 (2018) 209-220*
DOI: https://doi.org/10.12989/cac.2018.22.2.209

Effect of hybrid fibers on flexural performance of reinforced SCC symmetric inclination beams

Cong Zhang*[1,2], Zhihua Li[1] and Yining Ding[3]

[1]*School of Environment and Civil Engineering, Jiangnan University, Wuxi 214000, China*
[2]*Key Laboratory of Concrete and Pre-stressed Concrete Structure of Ministry of Education, Southeast University, Nanjing 210000, China*
[3]*State Key Laboratory of Coastal and Offshore Engineering, Dalian University of Technology, Dalian 116000, China*

(Received January 16, 2018, Revised June 10, 2018, Accepted June 15, 2018)

Abstract. In order to evaluate the effect of hybrid fibers on the flexural performance of tunnel segment at room temperature, twelve reinforced self-consolidating concrete (SCC) symmetric inclination beams containing steel fiber, macro polypropylene fiber, micro polypropylene fiber, and their hybridizations were studied under combined loading of flexure and axial compression. The results indicate that the addition of mono steel fiber and hybrid fibers can enhance the ultimate bearing capacity and cracking behavior of tested beams. These improvements can be further enhanced along with increasing the content of steel fiber and macro PP fiber, but reduced with the increase of the reinforcement ratio of beams. The hybrid effect of steel fiber and macro PP fiber was the most obvious. However, the addition of micro PP fibers led to a degradation to the flexural performance of reinforced beams at room temperature. Meanwhile, the hybrid use of steel fiber and micro polypropylene fiber didn't present an obvious improvement to SCC beams. Compared to micro polypropylene fiber, the macro polypropylene fiber plays a more prominent role on affecting the structural behavior of SCC beams. A calculation method for ultimate bearing capacity of flexural SCC symmetric inclination beams at room temperature by taking appropriate effect of hybrid fibers into consideration was proposed. The prediction results using the proposed model are compared with the experimental data in this study and other literature. The results indicate that the proposed model can estimate the ultimate bearing capacity of SCC symmetric inclination beams containing hybrid fibers subjected to combined action of flexure and axial compression at room temperature.

Keywords: tunnel segment; hybrid fiber; self-consolidating concrete; flexural loading; ultimate bearing capacity; cracking behavior; prediction model

1. Introduction

Fire usually poses serious damages to concrete shield tunnel segments: (a) spalling of concrete; (b) structural performance degradation of tunnel segments. Spalling of concrete during fire exposure will further aggravate these damages (Kim *et al*. 2013, Ibrahimbegovic *et al*. 2010, Ma *et al*. 2015), especially for high strength concrete (HSC) and self-consolidating concrete (SCC) due to their high compactness and low permeability (Bošnjak *et al*. 2013, Toropovs *et al.* 2015, Liu *et al.* 2008, Ye *et al.* 2007). Previous studies have confirmed the efficient roles of micro Polypropylene (PP) fiber on reducing the fire spalling risk of SCC (Mitsuo *et al.* 2012, Bangi and Horiguchi 2011, 2012). And the use of steel fiber can improve the structural performance of concrete element and tunnel segments during and after fire exposure (Ding *et al.* 2011, Carateli *et al.* 2011, Fuente *et al.* 2012, Plizzari and Tiberti 2006, Lee *et al.* 2014, Ramadoss and Nagamani 2012, 2013, Tuan *et al.* 2014, Kandasamy and Akila 2015). But the hybrid use of steel fiber and micro PP fiber in tunnel segment needs further investigation: (a) the aim of using micro PP fiber in tunnel segment is to improve the spalling resistance of concrete, but whether the micro PP fiber will affect the structural performance of SCC tunnel segment before and after fire exposure; (b) what's the manner of hybrid steel fiber and micro PP fiber affects the structural performance of tunnel segment before and after fire exposure? And whether there is a hybrid effect between steel fiber and micro PP fiber?

With the fast development of new construction materials, macro PP fiber for structural application has been produced and applied in structural elements more and more widely, especially for tunnel engineering owing to its excellent corrosion resistance (Oh *et al.* 2007, Nicola *et al.* 2011, Salah *et al.* 2009, Soutsos *et al.* 2012, Ponikiewski and Katzer 2014, Pujadas *et al.* 2014a, 2014b). The macro PP fiber is usually under a diameter of about 0.7 mm and a length of 45-60 mm. Previous studies demonstrate that the addition of macro PP fiber can significantly improve the mechanical performance of concrete elements. However, the following queries still needs further discussion: (a) whether the hybrid use of steel fiber and macro PP fiber will further improve the bearing capacity and cracking resistance of SCC tunnel segment before and after fire exposure; (b) what's the difference between macro PP fiber and micro PP fiber on affecting the structural performance of SCC tunnel segment before and after fire exposure?

*Corresponding author, Ph.D.
E-mail: zhangcong@jiangnan.edu.cn

ISSN: 1598-8198 (Print), 1598-818X (Online)

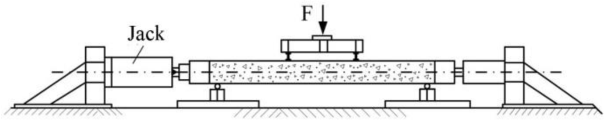

Fig. 1 Conventional simply supported beam with constant axial force by jacks

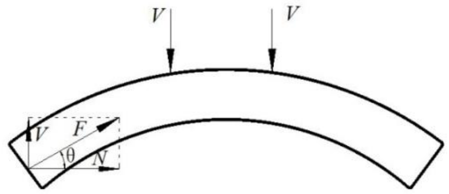

(a)

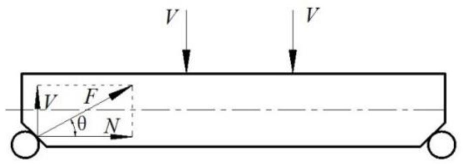

(b)

Fig. 2 Using symmetric inclination beam (b) to simulate the stress state of tunnel segment (a)

In the past, conventional simply supported beam with constant axial force on the two ends by using two jacks was usually employed to simulate the stress state of a tunnel segment, as showed in Fig. 1. But this type of beam can't reflect the change of axial force along with changing rock pressure and can't simulate the different central angle or curvature of actual tunnel segment. Recently, some researchers suggest using symmetric inclination beam to simulate the stress state of tunnel segment (Falkner and Henke 2004, Ding *et al.* 2014, Feyerabend 1995, Hemmy 2003), as shown in Fig. 2. An inclined support is employed instead of a vertical one. Compared to full-scale tunnel segment, the fabrication of symmetric inclination beam is more convenient and low-cost.

In this study, an inclination of 45^o was employed to simulate a tunnel segment with 90^o central angle. Flexural performance of twelve reinforced symmetric inclination beams containing steel fiber, micro PP fiber, macro PP fiber and their hybridizations were studied at room temperature. A calculation method for ultimate bearing capacity of flexural SCC symmetric inclination beams at room temperature by taking appropriate effect of hybrid fibers into consideration was proposed. Relevant studies for flexural SCC symmetric inclination beams with or without fibers after exposing to fire will be discussed in the follow-up papers.

2. Experiment

2.1 Materials

The raw materials used in this study were cement (P•O 52.5R), fly ash, quartz sand (0-5 mm) and crushed stone (5-15 mm). Their basic properties are showed in Table 1.

Table 1 Properties of raw materials

Materials	Density (g/cm^3)	Size	Mechanical property	Origin
 Cement	3.2	45μm sieve residue 14.16%	–	Dalian Onoda Cement Co. Ltd. , China
 Quartz sand	2.65	Fineness modulus 2.51 Medium sand	Moh's hardness 7	Dalian, China
 Fly ash	2.6	45 μm sieve residue 9.2%	–	Dalian, China

Table 2 Mix proportion of SCC without fibers /(kg/m^3)

Materials	Cement	Fly ash	Water	Sand 0-5 mm	Crushed stone 5-15 mm	Super plasticizer	W/B ratio
Content	400	160	180	764.8	832	6.72	0.32

Note: W/B is water to binder ratio (binder = cement + fly ash)

Table 3 Basic properties of different fibers used in this study

Materials	Density (g/cm^3)	Geometric size	Tensile strength (N/mm^2)	Quantity (pieces/kg)
Steel fiber	7.85	Hooked l_f =60 mm, d_f=0.75 mm	≥1100	4600
Micro PP fiber	0.91	Straight l_f =9 mm, d_f=18 μm	615	3.5 billion
Macro PP fiber	0.91	Double duoform l_f=45 mm, d_f=0.74 mm	465	50140

Table 4 Mechanical properties of steel reinforcement bars

Diameter /mm	Yield strength /MPa	Ultimate strength /MPa	Elongation /%	Elastic modulus /GPa
6.5 (stirrup)	278	320	21	210
8 (longitudinal)	491	651	13.5	200
10 (longitudinal)	475	643	8.5	200

Mix proportion of SCC without fibers is illustrated in Table 2. Fibers used in this study were steel fiber, micro polypropylene (PP) fiber, macro PP fiber and their combinations. Images and basic properties of different fibers employed in this paper are given in Fig. 3 and Table 3, respectively. Mechanical properties of steel reinforcement bars are showed in Table 4.

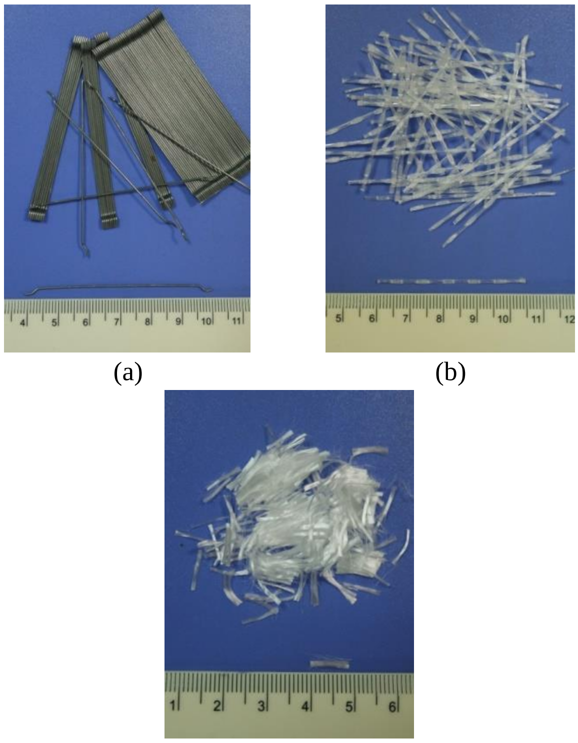

(a) (b)

(c)

Fig. 3 Fibers used in this study (a) Steel fiber; (b) Macro PP fiber; (c) Micro PP fiber

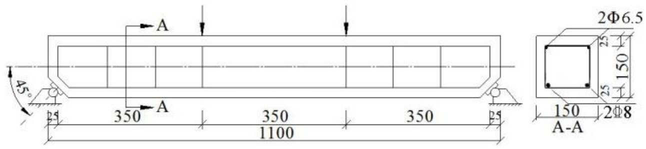

(a) Reinforcement ratio is 0.56%

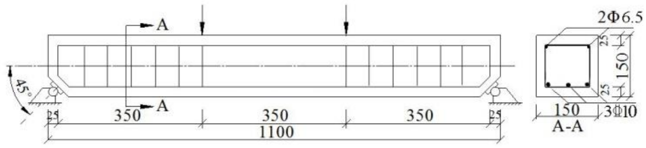

(b) Reinforcement ratio is 1.31%

Fig. 4 Geometry and reinforcement arrangement of test beams (Unit mm)

2.2 Design of specimen

All beams have the same dimension, as illustrated in Fig. 4. Reinforcement ratio and fiber content of the 12 series beams are showed in Table 5. Along with the casting of symmetric inclination beams, twelve 150 mm cubes were made for each mix group. And they were cured in 20°C water for 28d to determine the compressive strength of SCC and FRSCC using Weibull distribution method (Chen *et al.* 2016), as illustrated in Fig. 5, which takes the compressive strength of plain SCC as an example. And the compressive strength of all the series obtained by the Weibull distribution method is given in Table 5.

2.3 Loading program and measurement

Table 5 Reinforcement ratio and fiber content of simple supported beams

Beams	ρ_s /%	ρ_{sv} /%	Micro PP fiber/ (kg/m^3)	Steel fiber/ (kg/m^3)	Macro PP fiber /(kg/m^3)	f_c /MPa
SIB-1R	0.56	0.38 (120mm spacing)	0	0	0	63.2
SIB-2R	0.56	0.38 (120mm spacing)	0	30	0	66.7
SIB-3R	0.56	0.38 (120mm spacing)	1	20	0	63.5
SIB-4R	0.56	0.38 (120mm spacing)	0	20	6	68.4
SIB-5R	0.56	0.38 (120mm spacing)	0.5	20	3	65.1
SIB-6R	0.56	0.38 (120mm spacing)	0	50	0	65.3
SIB-7R	0.56	0.38 (120mm spacing)	1	40	0	67.3
SIB-8R	0.56	0.38 (120mm spacing)	0	40	4	64.5
SIB-9R	0.56	0.38 (120mm spacing)	0.5	40	2	62.2
SIB-10R	1.31	0.76 (60mm spacing)	0	0	0	63.2
SIB-11R	1.31	0.76 (60mm spacing)	0	30	0	66.7
SIB-12R	1.31	0.76 (60mm spacing)	0	20	6	68.4

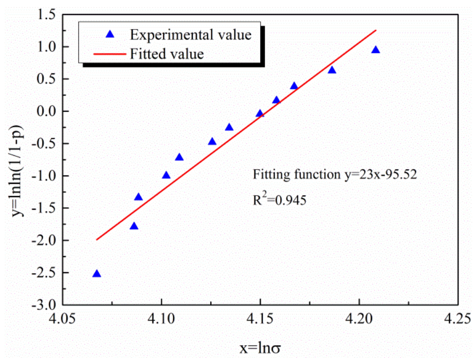

(a)

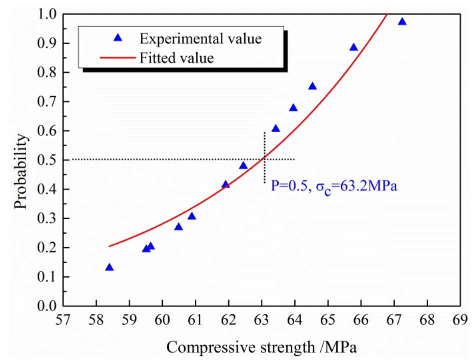

(b)

Fig. 5 Compressive strength test curves for plain SCC obtained by Weibull distribution

A displacement-controlled procedure was employed by using a hydraulic servo testing machine (maximum load capacity is 10000 N). In order to provide a pure flexural

Fig. 6 Loading and measuring arrangement of test beam

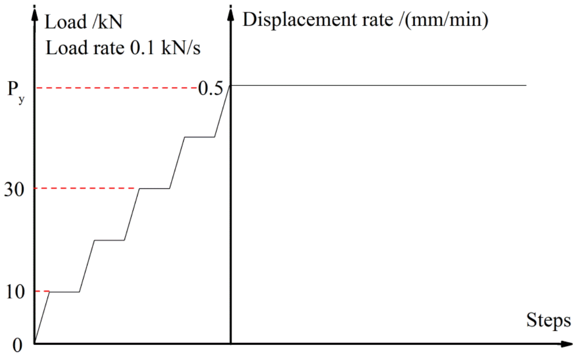

Fig. 7 Diagram of imposed load control and displacement control flexural test

zone, a steel distribution girder having 350 m spacing on the top face of the test beam was employed, as showed in Fig. 6.

The flexural test was performed through two steps, namely a load controlled step and displacement controlled step, as illustrated in Fig. 7. During the load controlled step, the load increment is 10kN and the load rate is 0.1 kN/s. After every loading step, the strain of steel rebar and the concrete crack patterns were recorded. When the bottom longitudinal reinforcement bars were yielded, the loading process was changed to displacement controlled stage. The displacement rate was 0.5mm/min until the beam failed. As illustrated in Fig. 6 and Fig. 8, three linear variable differential transducers (LVDTs) were employed to monitor the displacement of mid-span and loading points. Strain gauges (SG) were used to measure the strain of longitudinal reinforcement bars, as illustrated in Fig. 6.

3. Results and discussion

3.1 Load-deflection behavior

Fig. 9 shows the load-deflection behavior of SCC, FRSCC and HyFRSCC beams subjected to flexural loading. Table 6 gives the comparison of cracking load, yielding load and ultimate load for each group. It can be observed that the introduction of fibers brought a negligible effect on cracking load. But the yielding load and ultimate load of reinforced beams were much improved compared to that without any fibers. These improvements were further enhanced along with increasing the content of steel fiber and macro PP fiber, but reduced with the increase of reinforcement ratio of beams. The hybrid effect of steel

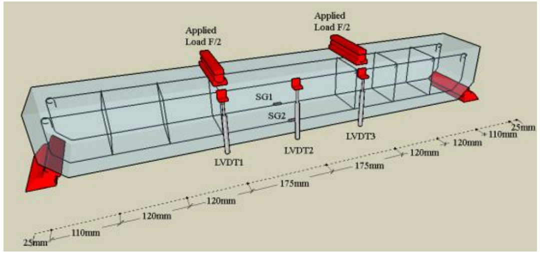

(a) 0.56% reinforcement ratio

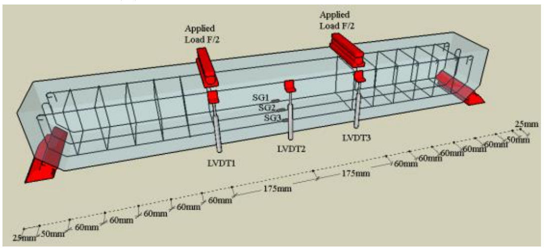

(b) 1.31% reinforcement ratio

Fig. 8 Schematic diagram for the arrangement of LVDTs and strain gauges

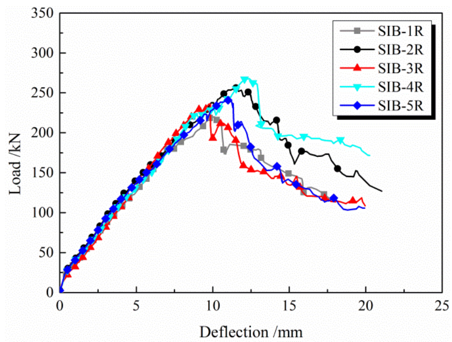

(a)

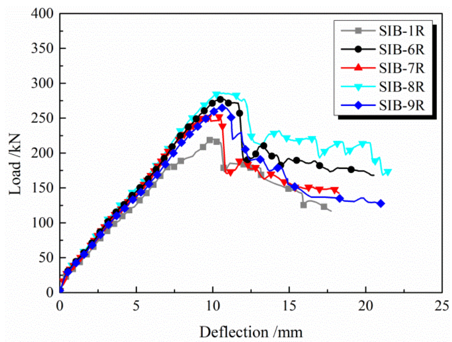

(b)

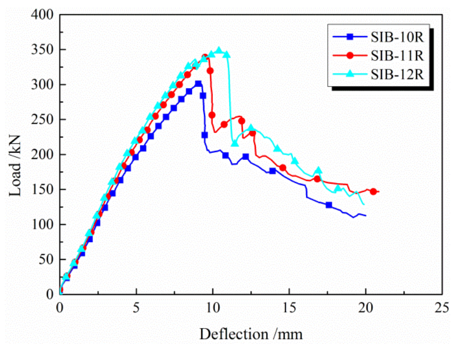

(c)

Fig. 9 Load-deflection behavior of reinforced SCC beams with or without fibers subjected to flexural loading

Table 6 Cracking load, yielding load, ultimate load and the corresponding deflection

Beams	Cracking load P_{cr} /kN	Yielding load $P_{y,b}$ /kN	Ultimate load $P_{u,b}$ /kN	Deflection at ultimate load $\delta_{u,b}$ /mm
SIB-1R	15	110	225	9.9
SIB-2R	16	127	255	11.5
SIB-3R	15	118	230	9.2
SIB-4R	16	135	267	12.2
SIB-5R	15	124	241	11.1
SIB-6R	18	148	276	10.7
SIB-7R	16	131	252	10.4
SIB-8R	17	155	286	10.8
SIB-9R	17	139	264	10.2
SIB-10R	21	181	302	9.1
SIB-11R	22	194	335	9.5
SIB-12R	21	207	349	10.3

fiber and macro PP fiber was the most obvious. However, the addition of micro PP fibers led to a degradation to the flexural performance of reinforced beams at room temperature. This may be related to the poor dispersion of fibers during the mix process, since the hybrid fibers containing micro PP fiber are very difficult to be well-distributed. Meanwhile, it also shows that although the addition of micro PP fiber can improve the fire resistance of concrete, it can't be employed to enhance the structural properties of reinforced beams. Compared to macro PP fiber and micro PP fiber, the steel fiber plays a dominant role on affecting the bearing capacity of reinforced beams.

Table 6 gives the test data of deflection at ultimate load. It can be seen that the addition of fibers increases the deflection of reinforced beams merely slightly owing to the existence of axial compression action. Compared to mono steel fiber, the hybridization of steel fiber and macro PP fiber can't further increase the beam deflection obviously. However, the effect of fibers on the deflection of reinforced beams is weakened along with the increase of reinforcement ratio.

3.2 Load-strain behavior of longitudinal reinforcement

Longitudinal reinforcement strain of all the beams was recorded automatically during the whole testing procedures, as illustrated in Fig. 10. It can be observed that the addition of fibers didn't bring a significant effect to the longitudinal reinforcement strain before cracking of the beams. After cracking, the longitudinal reinforcement strain of beams with fibers is lower than that of a beam without fiber at a given load level. It implies that the presence of fibers can reduce the stress of longitudinal reinforcement (Cattaneo *et al.* 2012, Dancygier and Savir 2006, Meda *et al.* 2012, Campione 2008). Compared to the beam with mono steel fibers, the diphasic use of steel fibers and PP fibers can further decrease the tensile strain of steel rebars. But the effect of fibers on reducing the longitudinal reinforcement strain is inconspicuous when the reinforcement ratio is 1.31%.

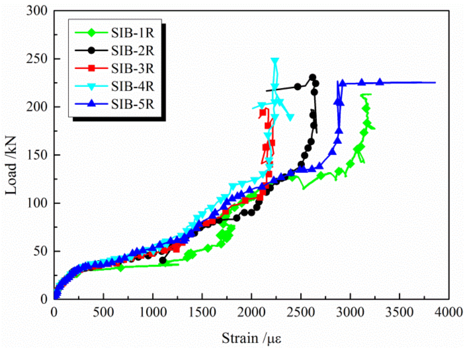

(a)

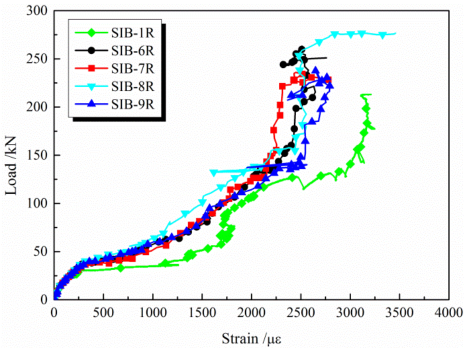

(b)

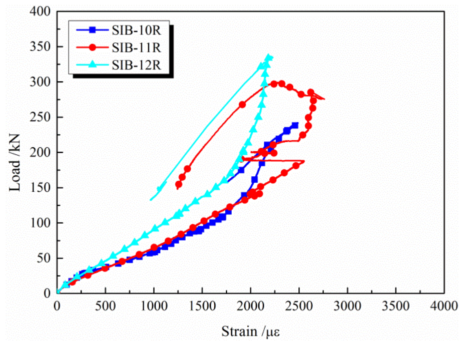

(c)

Fig. 10 Load-longitudinal reinforcement strain curves of simply supported beams with various fiber contents

3.3 Crack patterns

Fig. 11 gives the crack patterns of the tested beams during flexural loading. It can be noticed that cracks become smaller, narrower, closer and more diffused due to the inclusion of fibers. Steel fibers play a more predominant role than PP fibers in affecting the distribution of cracks. The addition of micro PP fiber can't bring a positive effect, even sometimes degradation, to the crack control ability of tested beams. It should be noticed that usually only one large crack was found on the beams containing micro PP fiber, which means the crack shows a localized phenomenon. Therefore, although the use of micro PP fiber can enhance the fire resistance of reinforced SCC beams, its detrimental effect on the structural performance at room temperature has to be taken into consideration. Moreover, the addition of high content steel fibers in flexural beams with low reinforcement ratio (e.g., 0.56% reinforcement ratio in this study) leads to a slower development of cracks.

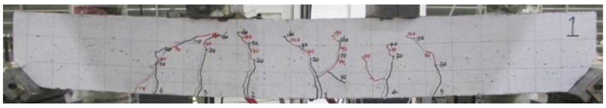

(a)

(b)

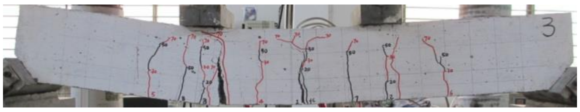

(c)

(d)

(e)

(f)

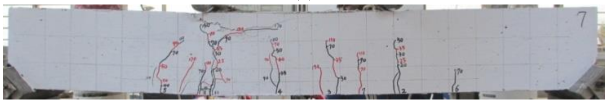

(g)

(h)

(i)

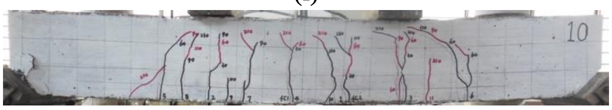

(j)

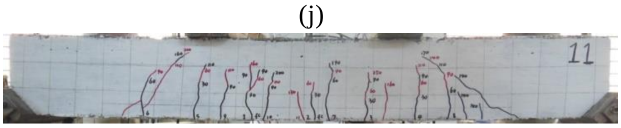

(k)

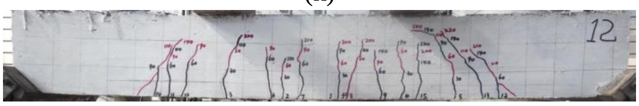

(l)

Fig. 11 Crack patterns of the tested symmetric inclination beams after unloading

3.4 Maximum crack width

Fig. 12 shows the development of maximum crack width for beams during flexural loading. The *X*-axis in Fig.

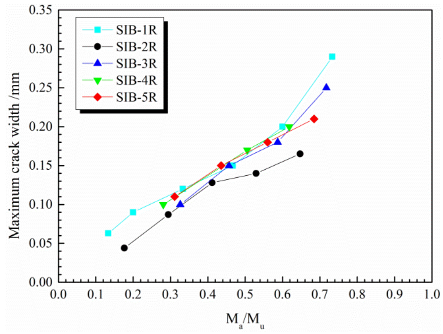

(a)

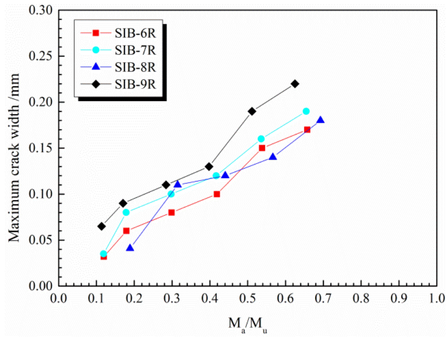

(b)

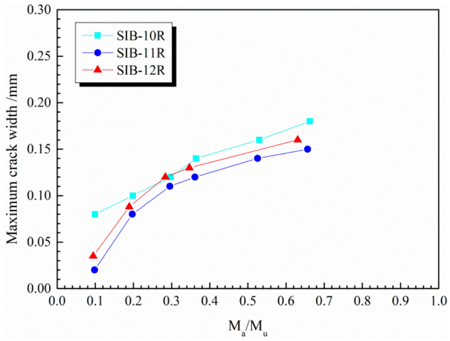

(c)

Fig. 12 Maximum crack width of reinforced SCC beams with or without fibers

12 is the ratio of immediate moment M_a and ultimate moment M_u. It can be observed that the effect of mono steel fibers in restricting crack width is better than that of hybrid fibers, which means the steel fiber plays a more predominant role than macro fibers and micro PP fibers in affecting the maximum crack width of reinforced SCC beams. From Fig. 12(a) and 12(c), it can be possible to conclude that increasing the reinforcement ratio is more effective in controlling crack width than increasing the fiber dosage.

3.5 Calculation of ultimate bearing capacity

To traditional reinforced concrete beams, the residual tensile strength of concrete in tension zone is generally neglected when calculating the flexural bearing capacity of beams. However, to reinforced concrete beams with fibers, the tensile strength of concrete after cracking needs to be considered. In this paper, the tensile stress of fiber σ_f in concrete beams is deduced firstly. And then the ultimate flexural bearing capacity of reinforced symmetric inclination beams with hybrid fibers is predicted based on σ_f. Finally, the prediction results used the proposed model are compared with the experimental data in this study and other literature.

3.5.1 Tensile stress of fiber σ_f

Based on probability statistics, the σ_f of fibers in concrete matrix can be expressed as Eq. (1).

$$\sigma_f = \frac{1}{2}\alpha V_f \bar{\sigma}_f (1+f_1) \tag{1}$$

where α is the fraction ratio of fibers which currently bridging the crack; V_f is the volume fraction of fibers; f_1 is the coefficient of friction between fiber and concrete matrix sheared over crack, taken as 1/3; $\bar{\sigma}_f$ is the average fiber stress for the load-carrying fibers, can be obtained by Eq. (2).

$$\bar{\sigma}_f = \frac{4\tau_f \bar{x}}{d_f} F_{be} \tag{2}$$

where τ_f is the interfacial shear stress between fiber and concrete, MPa, taken as 2.5 times of concrete tensile strength for hooked steel fiber (Voo and Foster 2003), and taken as 1.1 MPa for Double duoform macro PP fiber (Won *et al.* 2006); $\bar{x}$ is average shear length of fibers bridging over crack, mm, can be expressed as Eq. (3); d_f is the diameter of fiber, mm; F_{be} is fiber characteristics coefficient, taken as 1.2 to hooked steel fiber and 1.0 to smooth fibers.

$$\bar{x} = \frac{L_f}{4} \tag{3}$$

where L_f is fiber length, mm. Then, $\bar{\sigma}_f$ can be expressed as Eq. (4).

$$\bar{\sigma}_f = \tau_f \lambda F_{be} \tag{4}$$

where λ is the aspect ratio of fiber. Therefore, the σ_f can be expressed as Eq. (5).

$$\sigma_f = \frac{1}{2}\alpha \tau_f \lambda V_f F_{be}(1+f_1) \tag{5}$$

Relationship between crack width ω and α can be given as Eq. (6). And the ω can be expressed as Eq. (7).

$$\alpha = 1 - \omega \frac{2}{L_f} \tag{6}$$

$$\omega = \frac{4\tau_f \bar{x}}{E_f d_f} \tag{7}$$

Therefore, the σ_f can be rewritten as Eq. (8).

$$\sigma_f = \frac{1}{2}\tau_f \lambda V_f F_{be}(1+f_1) - \frac{\tau_f \lambda^2 V_f F_{be}}{E_f}(1+f_1) \tag{8}$$

The second part on the right side of Eq. (8) is negligible, so σ_f can be simplified as Eq. (9).

$$\sigma_f = \frac{1}{2}\tau_f \lambda V_f F_{be}(1+f_1) \tag{9}$$

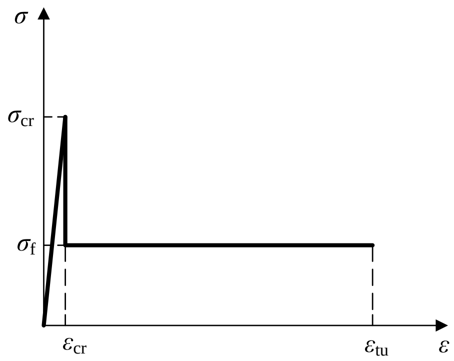

(a) Tension

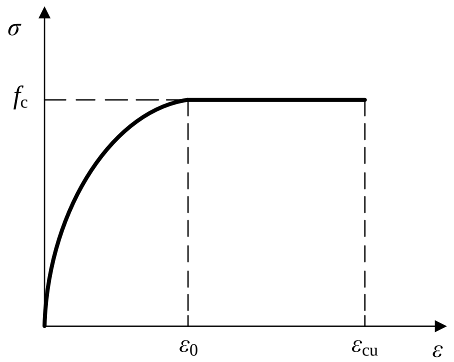

(b) Compression

Fig. 13 Stress-strain model for FRC

When taking the flexural loading into consideration, Eq. (9) can be rewritten as Eq. (10).

$$\sigma_f = \frac{1}{2}\tau_f \lambda V_f F_{be}(1+f_1)(1+f_2) \tag{10}$$

where f_2 is the flexural characteristics coefficient, expressed as Eq. (11).

$$f_2 = \frac{h-c}{L_0} \tag{11}$$

where h is the depth of the beam cross section, mm; c is the depth of neutral axis of reinforced concrete beam, mm; L_0 is the span of beam, mm.

3.5.2 Stress-strain model of materials

Tensile stress-strain model for concrete in tensile zone of beams is given as Eq. (12), as showed in Fig. 13(a).

$$\sigma_{ct} = \begin{cases} E_c \varepsilon_{ct} & 0 \le \varepsilon_{ct} \le \varepsilon_{cr} \\ \sigma_f & \varepsilon_{cr} < \varepsilon_s \le \varepsilon_{tu} \end{cases} \tag{12}$$

where ε_{cr} is the cracking strain of FRC, taken as 0.00015; ε_{tu} is the ultimate tensile strain of FRC, taken as 0.025.

Compressive stress-strain model for concrete in compressive zone of beams can be expressed as Eq. (13), as illustrated in Fig. 13(b).

$$\sigma_c = \begin{cases} f_c\left[1-\left(1-\dfrac{\varepsilon}{\varepsilon_0}\right)^2\right] & \varepsilon \le \varepsilon_0 \\ f_c & \varepsilon_0 \le \varepsilon \le \varepsilon_{cu} \end{cases} \tag{13}$$

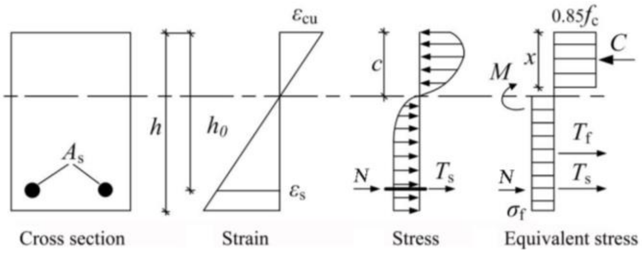

Fig. 14 Stress and strain distribution of FRC symmetric inclination beam containing conventional steel rebar

where f_c is the compressive strength of FRC, MPa; ε_0 is the compressive strain corresponding to f_c, taken as 0.002; ε_{cu} is the ultimate compressive strain, taken as 0.0035.

Stress-strain relationship of longitudinal rebar is given as Eq. (14).

$$\sigma_s = E_s \varepsilon_s \le f_y \tag{14}$$

where E_s is the elastic modulus of rebar, MPa; f_y is the yield strength of rebar, MPa; ε_s is the ultimate tensile strain of longitudinal rebar, taken as 0.01.

3.5.3 Ultimate bearing capacity

In the ultimate bearing capacity state, the flexural stress-strain distribution on the cross section of FRC beam containing conventional steel rebar can be illustrated as Fig. 14. Based on the plane cross-section assumption, equilibrium of force and equilibrium of moment, the ultimate bearing capacity of FRC beam can be expressed as Eq. (15) when taking the contribution of fibers into consideration.

$$M_u = \alpha_1 f_c bx(h_0 - \frac{x}{2}) - \sigma_f b(h-c)(\frac{h}{2} - \frac{c}{2} - \alpha_s) \tag{15}$$

where A_s is the steel reinforcement area, mm^2; h_0 is the effective height of beam cross section, mm; x is the depth of rectangular compressive stress blocks, mm; b is the width of the beam cross section, mm; h is the depth of the beam cross section, mm; c is the depth of neutral axis of reinforced concrete beam, mm;

The depth of neutral axis c of reinforced concrete beam and the depth of rectangular compressive stress blocks x can be obtained from Eqs. (16)- (18).

$$\alpha_1 f_c bx(c - \frac{x}{2}) = \frac{1}{2}\sigma_f b(h-c)^2 + f_y A_s(h_0 - c) + N_u(h_0 - c) \tag{16}$$

$$\alpha_1 f_c bx = f_y A_s + N_u + \sigma_f b(h-c) \tag{17}$$

$$x = 0.8c \tag{18}$$

To the reinforced SCC beams with steel fiber only, the σ_f can be given as Eq. (19).

$$\sigma_f = \frac{1}{2}\tau_{f,st}\lambda_{st}V_{f,st}F_{be,st}(1+f_1)(1+f_2) \tag{19}$$

where $\tau_{f,st}$ is the interfacial shear stress between steel fiber and concrete, MPa, taken as 2.5 times of concrete tensile strength for hooked steel fiber; λ_{st} is the aspect ratio of steel fiber; $V_{f,st}$ is the volume fraction of steel fiber; $F_{be,st}$ is the characteristics coefficient of steel fiber, taken as 1.2 to hooked steel fiber.

To the reinforced SCC beams with hybrid steel and macro PP fibers, the σ_f can be given as Eq. (20).

$$\sigma_f = \frac{1}{2}(1+f_1)(1+f_2)(\tau_{f,st}\lambda_{st}V_{f,st}F_{be,st} + \tau_{f,sy}\lambda_{sy}V_{f,sy}F_{be,sy}) \tag{20}$$

where $\tau_{f,sy}$ is the interfacial shear stress between macro PP fiber and concrete, MPa, taken as 1.1 MPa for Double duoform macro PP fiber; λ_{sy} is the aspect ratio of macro PP fiber; $V_{f,sy}$ is the volume fraction of macro PP fiber; $F_{be,sy}$ is the characteristics coefficient of macro PP fiber, taken as 1.2 to Double duoform macro PP fiber.

Due to the poor performance of micro PP fiber to structural behavior of reinforced concrete beams, the effect of micro PP fiber on the ultimate flexural bearing capacity of reinforced SCC beams is neglected in this paper.

3.5.4 Comparisons with test results

Table 7 and Fig. 15 illustrates the comparison of experimental and predicted ultimate flexural bearing capacity of the suggested model. It can be seen that the predicted moment is higher than experimental moment with a mean value of 1.116, a standard deviation of 0.098 and a coefficient of variation of 0.088. This may be because of

Table 7 Comparison of experimental results and predicted results for ultimate load capacity.

Beams	Steel fiber V_f /%	Macro PP fiber V_f /%	f_c /MPa	b /mm	h /mm	ρ_s /%	f_y /MPa	$M_{u,cal}$ /mm	$M_{u,exp}$ /mm	$M_{u,cal}$ / $M_{u,exp}$
SIB-1R	0	0	63.2	150	150	0.56	491	44.202	39.38	1.123
SIB-2R	0.385	0	66.7	150	150	0.56	491	46.088	44.63	1.033
SIB-3R	0.256	0	63.5	150	150	0.56	491	51.685	40.25	1.284
SIB-4R	0.256	0.659	68.4	150	150	0.56	491	55.554	46.73	1.189
SIB-5R	0.256	0.330	65.1	150	150	0.56	491	52.920	42.18	1.255
SIB-6R	0.641	0	65.3	150	150	0.56	491	52.318	48.30	1.083
SIB-7R	0.513	0	67.3	150	150	0.56	491	54.246	44.10	1.230
SIB-8R	0.513	0.439	64.5	150	150	0.56	491	51.833	50.05	1.036
SIB-9R	0.513	0.220	62.2	150	150	0.56	491	49.995	46.20	1.082
SIB-10R	0	0	63.2	150	150	1.31	475	56.880	52.85	1.076
SIB-11R	0.385	0	66.7	150	150	1.31	475	59.345	58.63	1.012
SIB-12R	0.256	0.659	68.4	150	150	1.31	475	60.972	61.08	0.998

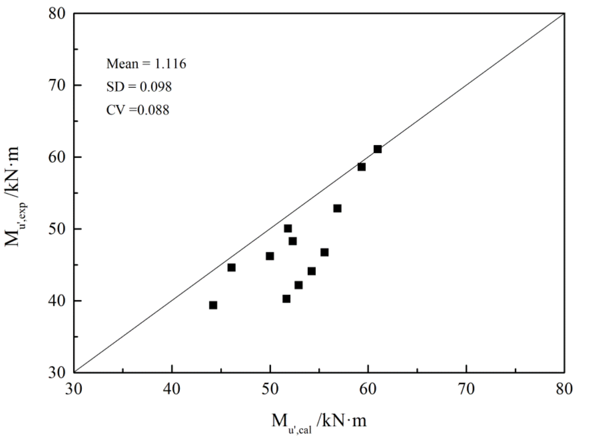

Fig. 15 Comparison of experimental results and predicted results using various models

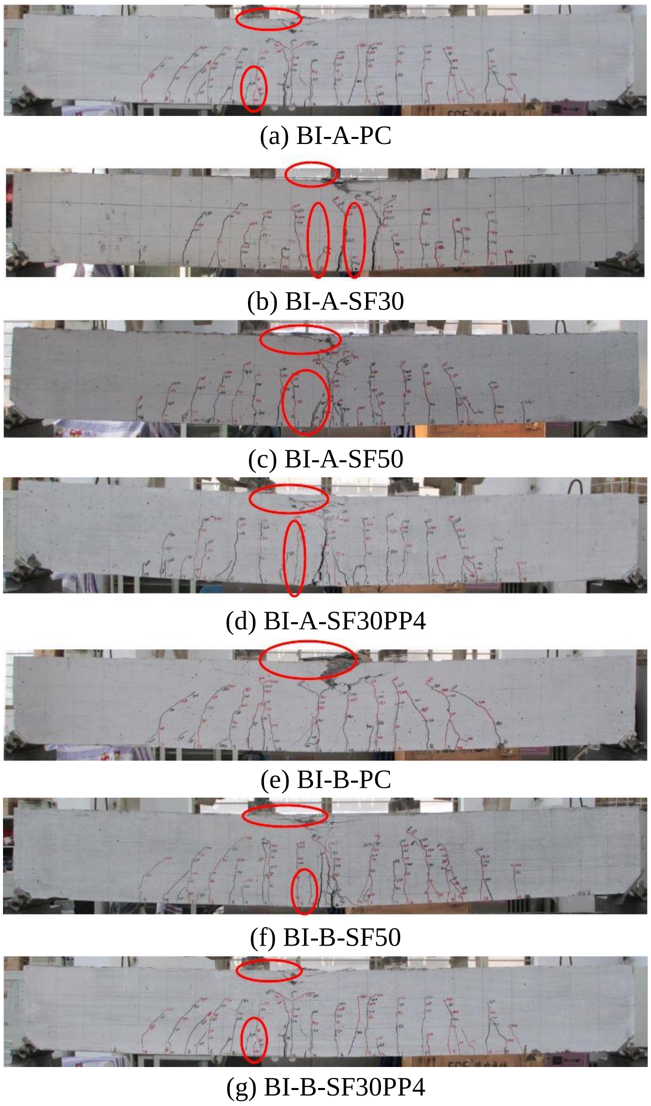

Fig. 16 Crack patterns of symmetric inclination beams of Ning's reserch containing hybrid fibers (Ning 2015)

not only the potential size effect of relatively small beams used in this study, but also relates to the orientation effect of fibers. In this calculation for the relatively small beams, the

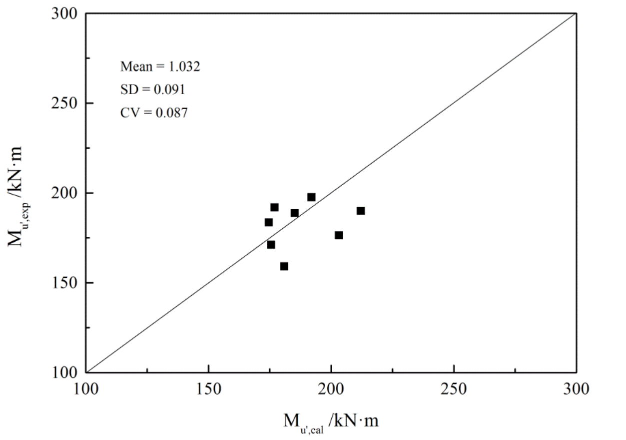

Fig. 17 Comparison of Ning's experimental results and predicted results using suggested model (Ning 2015)

distribution and orientation of fibers are a little overestimated (Pujadas *et al*. 2014c, 2014d, Alberti *et al*. 2015). Therefore, to extend the validity of the suggested model in this paper, the prediction to other experimental ultimate flexural bearing capacity results of reinforced symmetric inclination beams with fibers in previous literature is also made, as showed in Table 8, Fig. 16 and Fig. 17. It can be seen that the predicted moment and experimental moment are really close with a mean value of 1.032, a standard deviation of 0.091 and a coefficient of variation of 0.087. It may be said that the suggested model in this paper can be employed to the calculation of ultimate flexural bearing capacity of reinforced symmetric inclination beams with fibers.

4. Conclusions

The effects of steel fiber, micro PP fiber, macro PP fiber and their hybridization on the flexural performance of SCC symmetric inclination beams with different longitudinal reinforcement ratio at room temperature were investigated in this paper. The following conclusions can be drawn from this study.

- The addition of steel fibers can enhance the flexural bearing performance of reinforced SCC beams, and the hybrid use of steel fiber and macro PP fiber can bring a further improvement. But along with the increase of longitudinal reinforcement ratio, the above enhancement becomes not pronounced. Compared with macro PP fiber and micro PP fiber, the steel fiber plays a dominant role on affecting the bearing capacity of reinforced beams.
- The addition of fibers can decrease the strain, thus decrease the stress of longitudinal reinforcement. Mono steel fiber and the hybrid use of steel fiber and macro PP fiber present a significant effect on reducing the steel reinforcement strain and stress. Likewise, a higher longitudinal reinforcement ratio means a relatively lower fiber effect on steel rebars.
- Cracks of reinforced SCC symmetric inclination beams become smaller, narrower, closer and more

Table 8 Comparison of Ning's experimental results and the predicted results (Ning 2015)

Beams	Steel fiber V_f /%	Macro PP fiber V_f /%	f_c' /MPa	b /mm	h /mm	A_s /mm^2	f_y /MPa	$M_{u,cal}$ /mm	$M_{u,exp}$ /mm	$M_{u,cal}$ / $M_{u,exp}$
BI-A-PC	0	0	68.5	200	300	402	471	185.230	188.8	0.981
BI-A-SF30	0.385	0	70.3	200	300	402	471	176.926	192.0	0.921
BI-A-SF30PP4	0.385	0.439	70.1	200	300	402	471	174.599	183.6	0.951
BI-A-SF50	0.641	0	73.0	200	300	402	471	175.541	171.2	1.025
BI-B-PC	0	0	69.0	200	300	509	454	203.167	176.4	1.152
BI-B-SF30PP4	0.385	0.439	70.1	200	300	509	454	192.012	197.6	0.972
BI-B-SF50	0.641	0	68.7	200	300	509	454	180.940	159.2	1.137
BI-C-PC	0	0	67.0	200	300	628	443	212.165	190.0	1.117

diffused due to the inclusion of fibers. Steel fibers play a more predominant role than PP fibers, but lead to a slower development of cracks. The addition of micro PP fiber can't bring a positive effect, even sometimes degradation, to the crack control ability of tested beams. Mono steel fibers in restricting crack width are better than that of hybrid fibers. Increasing the reinforcement ratio is more effective in controlling crack width than increasing the fiber dosage.

• A calculation model for ultimate bearing capacity of SCC symmetric inclination beams at room temperature was suggested. The model considers the contribution of hybrid fibers to SCC in tension zone by taking into account the stress transfer behavior of different fibers. The results of the proposed model are found to agree well with experimental data in this study and other literature. The proposed model can be employed to estimate the ultimate flexural bearing capacity of reinforced SCC symmetric inclination beams containing hybrid fibers at room temperature.

Acknowledgements

The authors gratefully acknowledge the Foundation Research Project of Jiangsu Province (The Natural Science Fund NO. BK20170192) and the Open Foundation of Key Laboratory of Concrete and Pre-stressed Concrete Structure of Ministry of Education (CPCSME2016-10).

References

Alberti, M.G., Enfedaque, A. and Galvez, J.C. (2015), "Comparison between polyolefin fibre reinforced vibrated conventional concrete and self-compacting concrete", *Constr. Build. Mater.*, **85**, 182-194.

Bangi, M.R. and Horiguchi, T. (2011), "Pore pressure development in hybrid fibre-reinforced high strength concrete at elevated temperatures", *Cement Concrete Res.*, **41**, 1150-1156.

Bangi, M.R. and Horiguchi, T. (2012), "Effect of fiber type and geometry on maximum pore pressures in fiber-reinforced high strength concrete at elevated temperatures", *Cement Concrete Res.*, **42**, 459-466.

Bošnjak, J., Ožbolt, J. and Hahn, R. (2013), "Permeability measurement on high strength concrete without and with polypropylene fibers at elevated temperatures using a new test setup", *Cement Concrete Res.*, **53**, 104-111.

Campione, G. (2008), "Simplified flexural response of steel fiber-reinforced concrete beams", *J. Mater. Civil Eng.*, **20**(4), 283-293.

Caratelli, A., Meda, A., Rinaldi, Z. and Romualdi, P. (2011), "Structural behaviour of precast tunnel segments in fiber reinforced concrete", *Tunn. Undergr. Sp. Tech.*, **26**(2), 284-291.

Cattaneo, S., Giussani, F. and Mola, F. (2012), "Flexural behaviour of reinforced, prestressed and composite self-consolidating concrete beams", *Constr. Build. Mater.*, **36**, 826-837.

Chen, X., Ge, L., Yuan, H. and Zhou, J. (2016), "Effect of prestatic loading on dynamic tensile strength of concrete under high strain rates", *J. Mater. Civil Eng.*, **28**(12), 1-7.

Dancygier, A.N. and Savir, Z. (2006), "Flexural behavior of HSFRC with low reinforcement ratios", *Eng. Struct.*, **28**(11), 1503-1512.

De la Fuente, A., Pujadas, P., Blanco, A. and Aguado, A. (2012), "Experiences in Barcelona with the use of fibres in segmental linings", *Tunn. Undergr. Sp. Tech.*, **27**(1), 60-71.

Ding, Y., Liu, H., Pacheco-Torgal, F. and Jalali, S. (2011), "Experimental investigation on the mechanical behaviour of the fiber reinforced high-performance concrete tunnel segment", *Compos. Struct.*, **93**(4), 1284-1289.

Falkner, H. and Henke, V. (2004), "SFRC-shear load bearing capacity and tunnel linings", *Proceedings of the 6th Rilem Symposium on Fiber-Reinforced Concrete*, Varenna, Italy.

Feyerabend, B. (1995), "Zum Einfluss verschiedener Stahlfasern auf das Verformungs und Rissverhalten von Stahlfaserbeton unter den Belastungsbdingungen einer Tunnelschale", No. 95-8, Ruhr Universitaet Bochum Institut fuer Konstruktiven Ingenieurbau, Ruhr, Germany.

Hemmy, O. (2003), "Zum Gebrauchs-Und Tragverhalten von Tunnelschalen aus Stahlfaserbenton und Stahfaserverstaerktem Stahlbeton", Ph.D. Dissertation, Technischen Universitaet Braunschweig, Braunschweig, Germany.

Ibrahimbegovic, A., Boulkertous, A., Davenne, L., Muhasilovic, M. and Pokrklic, A. (2010), "On modeling of fire resistance tests on concrete and reinforced-concrete structures", *Comput. Concrete*, **7**(4), 285-301.

Kandasamy, S. and Akila, P. (2015), "Experimental analysis and modeling of steel fiber reinforced SCC using central composite design", *Comput. Concrete*, **15**(2), 215-229.

Kim, H.J., Kim, H.Y., Kwon, I.K., Kwon, K.H., Min, B.Y. and Cho, B.Y. (2013), "A study on the fire performance and heat transfer of the HPC column with fiber-cocktail in ISO fire under loading condition", *Comput. Concrete*, **12**(5), 717-737.

Lee, D.H., Hwang, J.H., Ju, H. and Kim, K.S. (2014), "Application of direct tension force transfer model with modified fixed-angle softened-truss model to finite element analysis of steel fiber-reinforced concrete members subjected to shear", *Comput. Concrete*, **13**(1), 49-70.

Liu, X., Ye, G. and Schutter, G.D. (2008), "On the mechanism of Polypropylene fibers in preventing fire spalling in self-

compacting and high-performance cement paste", *Cement Concrete Res.*, **38**, 487-499.
Ma, Q., Guo, R., Zhao, Z., Lin, Z. and He, K. (2015), "Mechanical properties of concrete at high temperature-A review", *Constr. Build. Mater.*, **93**, 371-383.
Meda, A., Minelli, F. and Plizzari, G.A. (2012), "Flexural behaviour of RC beams in fibre reinforced concrete", *Compos. Part B-Eng.*, **43**(8), 2930-2937.
Mitsuo, O., Shinya, U. and Toshiro, K. (2012), "Study of mechanisms of explosive spalling in high-strength concrete at high temperatures using acoustic emission", *Constr. Build. Mater.*, **37**, 621-628.
Nicola, B., Claudio, M. and Marco, S. (2011), "Post-cracking behaviour of steel and macro-synthetic fibre-reinforced concretes", *Constr. Build. Mater.*, **25**, 2713-2722.
Ning, X.L. (2015), "Bending capacity and cracking behavior of fiber reinforced self-consolidating concrete beams containing conventional reinforcement", Ph.D. Dissertation, Dalian University of Technology, Dalian, China.
Oh, B.H., Kim, J.C. and Choi, Y.C. (2007), "Fracture behavior of concrete members reinforced with structural synthetic fibers", *Eng. Fract. Mech.*, **74**, 243-257.
Plizzari, G.A. and Tiberti, G. (2006), "Steel fibers as reinforcement for precast tunnel segments", *Tunn. Undergr. Sp. Tech.*, **21**(3), 438-439.
Ponikiewski, T. and Katzer, J. (2014), "Properties of fresh SCC mix reinforced by different types of steel and polymer fibre", *Constr. Build. Mater.*, **62**, 96-101.
Pujadas, P., Blanco, A., Cavalaro, S. and Aguado, A. (2014), "Plastic fibres as the only reinforcement for flat suspended slabs: experimental investigation and numerical simulation", *Constr. Build. Mater.*, **57**, 92-104.
Pujadas, P., Blanco, A., Cavalaro, S., de la Fuente, A. and Aguado, A. (2014), "Fibre distribution in macro-plastic fibre reinforced concrete slab-panels", *Constr. Build. Mater.*, **64**, 496-503.
Pujadas, P., Blanco, A., Cavalaro, S.H.P., Aguado, A., Grünewald, S., Blom, K. and Walraven, J.C. (2014), "Plastic fibres as the only reinforcement for flat suspended slabs: Parametric study and design considerations", *Constr. Build. Mater.*, **70**, 88-96.
Pujadas, P., Blanco, A., Cavalaro, S.H.P., De La Fuente, A. and Aguado, A. (2014), "Multidirectional double punch test to assess the post-cracking behaviour and fibre orientation of FRC", *Constr. Build. Mater.*, **58**, 214-224.
Ramadoss, P. and Nagamani, K. (2012), "Statistical methods of investigation on the compressive strength of high-performance steel fiber reinforced concrete", *Comput. Concrete*, **9**(2), 153-169.
Ramadoss, P. and Nagamani, K. (2013), "Stress-strain behavior and toughness of high-performance steel fiber reinforced concrete in compression", *Comput. Concrete*, **11**(2), 149-167.
Salah, A., Ardavan, Y. and Rieder, K.A. (2009), "Shear behavior of macro-synthetic fiber-reinforced concrete beams without stirrups", *ACI Mater. J.*, **106**(4), 381-389.
Soutsos, M.N., Le, T.T. and Lampropoulos, A.P. (2012), "Flexural performance of fibre reinforced concrete made with steel and synthetic fibres", *Constr. Build. Mater.*, **36**, 704-710.
Toropovs, N., Monte, F.L., Wyrzykowski, M., Weber, B., Sahmenko, G., Vontobel, P., ... and Lura, P. (2015), "Real-time measurements of temperature, pressure and moisture profiles in high-performance concrete exposed to high temperature during neutron radiography imaging", *Cement Concrete Res.*, **68**, 166-173.
Tuan, B.L.A., Tesfamariam, M.G., Hwang, C.L., Chen, C.T., Chen, Y.Y. and Lin, K.L. (2014), "Effect of fiber type and content on properties of high-strength fiber reinforced self-consolidating concrete", *Comput. Concrete*, **14**(3), 299-313.
Voo, J. and Foster, S. (2003), "Variable engagement model for fibre reinforced concretein tension", UNICIV Report No. R-420, The University of New South Wales, Sydney, Australia.
Won, J.P., Lim, D.H. and Park, C.G. (2006), "Bond behaviour and flexural performance of structural synthetic fiber-reinforced concrete", *Mag. Concrete. Res.*, **58**, 401-410.
Ye, G., Liu, X. and Schutter, G.D. (2007), "Phase distribution and microstructural changes of self-compacting cement paste at elevated temperature", *Cement Concrete Res.*, **37**, 978-987.
Yining, D., Hekai, L., Yulin, Z., Xiliang, N. and Azevedo, C.M. (2014), "Shear resistance and cracking behaviour of SFRC beams with and without axial load", *Mag. Concrete. Res.*, **66**(23), 1183-1193.

CC

Nomenclature

ρ_s	Longitudinal reinforcement ratio
ρ_{sv}	stirrupt reinforcement ratio
SF	steel fiber
PPF	polypropylene fiber
P_{cr}	cracking load
$P_{y,b}$	yielding load
$P_{u,b}$	ultimate load
$\delta_{u,b}$	deflection of simply suported beam at ultimate load
σ_f	tensile stress of fibers
α	fraction ratio of fibers which currently bridging the crack
V_f	volume fraction of fibers
$V_{f,st}$	volume fraction of steel fiber
$V_{f,sy}$	volume fraction of macro PP fiber
f_1	coefficient of friction between fiber and concrete matrix sheared over crack
f_2	flexural characteristics coefficient
$\bar{\sigma}_f$	average fiber stress for the load-carrying fibers
τ_f	interfacial shear stress between fiber and concrete
$\tau_{f,st}$	interfacial shear stress between steel fiber and concrete
$\tau_{f,sy}$	interfacial shear stress between macro PP fiber and concrete
$\bar{x}$	average shear length of fibers bridging over crack
d_f	diameter of fiber
F_{be}	fiber characteristics coefficient
$F_{be,st}$	characteristics coefficient of steel fiber
$F_{be,sy}$	characteristics coefficient of macro PP fiber
L_f	fiber length
λ	aspect ratio of fiber
λ_{st}	aspect ratio of steel fiber
λ_{sy}	aspect ratio of macro PP fiber
ω	crack width
h	depth of the beam cross section
c	depth of neutral axis of reinforced concrete beam
L_0	span of beam
ε_{cr}	cracking strain of FRC
ε_{tu}	ultimate tensile strain of FRC
f_c	compressive strength of FRC
ε_0	compressive strain corresponding to compressive strength
ε_{cu}	ultimate compressive strain

E_s elastic modulus of rebar
f_y yield strength of rebar
ε_s ultimate tensile strain of longitudinal rebar
A_s steel reinforcement area
h_0 effective height of beam cross section
x depth of rectangular compressive stress blocks
b width of the beam cross section
h depth of the beam cross section
c depth of neutral axis of reinforced concrete beam
M_{pre} Predicted moment
M_{exp} Measured moment